2-15-2015

Dynamics of poly(methyl methacrylate)–montmorillonite nanocomposites: A dielectric study

Weixing Sun
Iowa State University

Li Li
Iowa State University

Michael R. Kessler
Washington State University

Nicola Bowler
Iowa State University, nbowler@iastate.edu

This article is a post-print copy of W. Sun, L. Li, E. A. Stefanescu, M. R. Kessler, N. Bowler: Dynamics of Poly(methyl methacrylate)-Montmorillonite Nanocomposites: A Dielectric Study, *Journal of Non-Crystalline Solids*, 2015, 410, 43-50. doi:10.1016/j.jnoncrysol.2014.11.030.

Dynamics of poly(methyl methacrylate)–montmorillonite nanocomposites: A dielectric study

Weixing Sun[a],
Li Li[a],
Eduard A. Stefanescu[a],
Michael R. Kessler[b],
Nicola Bowler[a]

[a] Department of Materials Science and Engineering, Iowa State University, Ames, IA 50011, USA
[b] School of Mechanical and Materials Engineering, Washington State University, Pullman, WA 99164, USA

Abstract

The effect of varying amounts of montmorillonite (MMT) filler (in weight ratios of 100/0, 100/5, and 100/10) on the molecular dynamics and polarization of atactic poly(methyl methacrylate) (PMMA) is investigated using broad-band dielectric spectroscopy from 10^{-2} to 10^{6} Hz and at temperatures from 30 to 140 °C. The experimental data were analyzed with the sum of Havriliak–Negami (HN) functions and a power-law conduction term. The characteristic frequency, activation energies, and dielectric strength of PMMA/MMT nanocomposites were analyzed. As MMT content increases, a Maxwell–Wagner–Sillars (MWS) relaxation emerges in the nanocomposites and the α-relaxation contributed by main-chain movements above T_g occurs at lower temperatures as silicate layers in MMT segregate PMMA chains into smaller domains. The characteristic frequency of β-relaxations is influenced by the mergence with the α-relaxation above T_g. Further, the strength of the β-relaxation is stable as a function of temperature in both pure PMMA and the PMMA/MMT nanocomposites whereas, in the nanocomposites, the strengths of the α- and MWS relaxations increase significantly with temperature up to approximately 120 °C.

Keywords

- PMMA/MMT nanocomposites;
- Dielectric spectroscopy;
- Havriliak–Negami model;
- Relaxation strength

1. Introduction

Polymer nanocomposites can be defined as multiphase materials with nanoscale filler particles (nanofiller) dispersed in a continuous polymer matrix. Even a small loading of nanofiller – which

generally exhibits remarkably larger surface area than micrometer-sized fillers of the same volume fraction – can give rise to strong interactions with the polymer matrix [1]. Consequently, nanocomposite materials containing various nanofillers, particularly those containing high aspect-ratio nanofillers, have significantly improved physical characteristics, such as increased tensile strength, resistance to dielectric breakdown, and improved thermal behavior compared with the unfilled polymer, without demanding any significant change in required processing techniques. Polymers reinforced with clay, silica, rutile, or alumina nanoparticles have been shown to exhibit excellent dielectric properties [2] and [3]. In this paper, the molecular dynamics of poly(methyl methacrylate)/montmorillonite (PMMA/MMT) nanocomposites are investigated by dielectric spectroscopy.

PMMA is an amorphous thermoplastic polymer possessing high strength, superior dimensional stability, and excellent resistance to wear. Because of these properties it is employed in many outdoor applications, such as aircraft windows, lighthouse lenses, and spectator protection in ice hockey rinks. Additionally, flexible PMMA films have been used as solar modules in the solar cell industry. The molecular dynamics of PMMA have been studied in many previous works, including [4], [5], [6] and [7]. The glass transition temperature, T_g, of PMMA can range from 85 to 165 °C. The α-relaxation of PMMA is associated with motions of the main polymer chains and occurs at and above T_g, while its β-relaxation is caused by the hindered rotation of the methacrylate side group [4] and [8]. Among various inorganic additives that have been explored (including, for example, silicon oxides, metal oxides, nanoclay, and carbon nanotubes), montmorillonite (MMT), a clay mineral, is the most commonly used filler. The silicate aggregate layers of MMT can be dispersed on a nanometer level in an engineering polymer and can be more easily intercalated or exfoliated with various polymers [1], [9] and [10]. MMT exhibits a sandwich-structure of silicate layers. The fundamental units are platelets whose thickness ranges from approximately 1 to 2.4 nm and whose lateral dimensions range from approximately 100 nm to 10 μm [9] and [11]. Stacking of the platelets leads to a regular van der Waals gap between the layers called the interlayer or gallery, where exchangeable cations are located.

The effect of MMT nanofillers on dielectric permittivity is associated with interfacial polarization and low-frequency electrical conduction mechanisms. Even a small fraction of nanofillers contains a sufficiently large number of particles generating a considerable surface area to interact with a significant number of polymer chains in the nanocomposite, as has been reported in studies on other polymers filled with MMT, namely polypropylene/MMT [12] and polyvinylidene fluoride (PVDF)/MMT [10]. The introduction of MMT has been shown to increase the real permittivity of the polymer–MMT nanocomposite and to introduce a new dielectric loss peak, corresponding to interfacial polarization (also known as Maxwell–Wagner–Sillars (MWS) polarization). Apart from giving rise to MWS relaxation, the addition of MMT nanoparticles has also been observed to influence the molecular relaxations of the polymer matrix [13] and [14]. It is noteworthy that a frozen dynamics has been associated with the layer of amorphous polymer neighboring a crystalline region in semicrystalline block copolymers [15] and [16]. This mechanism is another possible contributor to the observed behavior in this PMMA–MMT system.

In this work, PMMA composites with a mixture of exfoliated and intercalated MMT nanoparticles were prepared in weight ratios of 100/0, 100/5 and 100/10 of PMMA/MMT. The

nanocomposites were characterized by various methods of material analysis such as thermogravimetric analysis (TGA), differential scanning calorimetry (DSC), transmission electron microscopy (TEM), and X-ray diffraction (XRD). The dielectric complex permittivity of the samples was measured at a voltage of 1 V (typical for measurements with the Novocontrol Alpha-A dielectric spectrometer), over a frequency range from 10^{-2} to 10^{6} Hz, at temperatures from 30 to 140 °C. The dielectric relaxations and low-frequency conduction of the nanocomposites often merge together over certain frequency and temperature ranges. In order to separate individual relaxations from low-frequency conduction, a sum of Havriliak–Negami (HN) functions were applied in order to elucidate the frequency-dependence of the polymer molecular relaxations (α- and β-) and the MWS relaxation, and a power-law relation was used to describe the low-frequency conduction [17]. The effects of MMT content on the molecular dynamics and polarization of the nanocomposites were then analyzed.

2. Experiment

The methylmethacrylate (MMA) monomer (99%, stabilized) employed in all experiments was purchased from Acros Organics. The radical initiator, benzoyl peroxide, BPO, (97% dry weight) was obtained from Alfa Aesar. The MMT clay (Cloisite 20A) was provided by Southern Clay Products (Gonzales, TX, USA). Cloisite 20A is a Na-MMT modified with dimethyl dehydrogenated tallow ammonium, which imparts hydrophobicity and increases the number of inter-platelet galleries. The clay platelets have a thickness of 1 nm and equivalent diameters ranging from 100 nm to approximately 10 μm. According to the manufacturer's information: 10% of the particles have diameter less than 2 μm, 50% less than 6 μm, and 90% less than 10 μm. Thermogravimetric analysis (TGA) was conducted in order to determine the water content of the MMT nanoclay on a Thermal Analysis (TA) Instruments Q50 thermobalance. The weight change of MMT was monitored while the nanoclay was heated from 20 to 800 °C at a heating rate of 20 °C/min.

Prior to nanocomposite fabrication the nanoclay was dried in a furnace at 80 °C for 2 h to eliminate MMT surface moisture. The stabilizing inhibitor was removed from MMA by washing the monomer three times with a 10% NaOH aqueous solution, followed by three washes with distilled water. The purified monomer was dried using molecular sieves. The first step in the composite preparation was the dissolution of initiator in the monomer, followed by the addition of the filler (MMT). The molar ratio MMA/BPO was maintained at $1/(2 \times 10^{-3})$ in all systems, and the MMA/MMT weight ratios were 100/5 and 100/10. The corresponding weight fraction and volume fraction of MMT for each sample are shown in Table 1. In the following discussions the two nanocomposite samples are designated as '5MMT' and '10MMT', respectively. The mixtures were sonicated at 0.20 W and mixed at 1–2 minute intervals employing a Fisher Scientific Model 100 sonic dismembrator. Following the sonication, systems were centrifuged for approximately 1 min to remove possible air bubbles. The sequence of sonication followed by mixing and centrifugation was repeated five times for each sample. The in-situ polymerization of the two systems was carried out in an oven at 80 °C overnight. This procedure resulted in binary nanocomposites with a number-average chain length of PMMA of approximately 7.7 k, which was determined by a Gel Permeation Chromatography (GPC) test. This relatively low molecular weight material is useful in applications where flexibility is advantageous such as in flexible solar cell technology and for coatings with good gas- and liquid-barrier properties. A pure

PMMA sample was prepared by the same in-situ polymerization procedure, as a control sample. Atactic and completely amorphous PMMA was synthesized in the radical polymerization to eliminate the effect of tacticity for all three samples.

Table 1.
Compositions of PMMA/MMT nanocomposites.

Sample	MMT weight fraction (%)	MMT volume fraction (%)
PMMA	0	0
5MMT	4.80 ± 0.05	2.40 ± 0.02
10MMT	9.10 ± 0.10	4.80 ± 0.05

Transmission electron microscopy (TEM) was employed to investigate the MMT dispersion in 5MMT and 10MMT using a JEOL 2100 200 kV microscope. Wide angle X-ray diffraction (WAXD) tests were conducted to estimate the spacing of intercalated silicate layers of MMT in 5MMT and 10MMT using a Siemens D-500 Bruker AXS X-ray diffractometer. Differential scanning calorimetry (Q20, TA Instruments, USA) was conducted to determine the onset T_g of pure PMMA at a heating rate of 10 °C/min. The complex permittivity of the three samples (PMMA, 5MMT, and 10MMT) was measured using a Novocontrol Dielectric Spectrometer (Novocontrol Technologies, Germany) in which the sample cell consisting of 20-mm-diameter parallel plate electrodes, was housed in a temperature-controlled chamber. The overall uncertainty in measured permittivity is estimated to be around 1%, introduced by the sample thickness variance and the error of the analyzer. The measurement was carried out at a voltage of 1 V, over a frequency range from 10^{-2} to 10^{6} Hz and temperatures from 30 to 140 °C in 10 °C increments. The upper temperature limit was chosen to be 20 °C below the softening temperature of PMMA, which is approximately 160 °C.

3. Results

Results of the TGA test for nanoclay moisture content are shown in Fig. 1. The weight loss up to 100 °C is approximately 2.4% indicating the amount of moisture in MMT. MMT was therefore dried at 80 °C to remove moisture prior to composite fabrication. The additional weight loss of approximately 6% observed in the temperature interval from 100 to 650 °C corresponds to the combustion of hydrocarbon functional chains present at the surface of Cloisite 20A clay platelets. The dispersion of clay platelets in 5MMT and 10MMT samples is displayed in the TEM images of Fig. 2. As shown in Fig. 2a and c, the nanoclay particles in 5MMT and 10MMT are homogenously dispersed and randomly oriented. Fig. 2b and d reveals the presence of both intercalated and exfoliated silicate layers of MMT in the PMMA matrix. Compared with 5MMT, silicate layers in 10MMT appear to be more severely intercalated. The spacing between intercalated silicate layers of MMT in 5MMT and 10MMT is calculated using Bragg's law:

$$\lambda = 2d\sin\theta$$

where λ is the wavelength of the X-rays used (0.154 nm for the copper target used to generate X-rays in these tests), d is the spacing between the silicate layers, and θ is the angle between the incident X-rays and the scattering planes. The increment of θ in the XRD tests was selected to be 0.05°, Fig. 3. A peak in the spectra at $2\theta = 2.5°$ indicates that the spacing between the MMT silicate layers in the two nanocomposites is 3.5 nm, increased by 40% compared with pure MMT, caused by the intercalation of PMMA chains between the silicate layers.

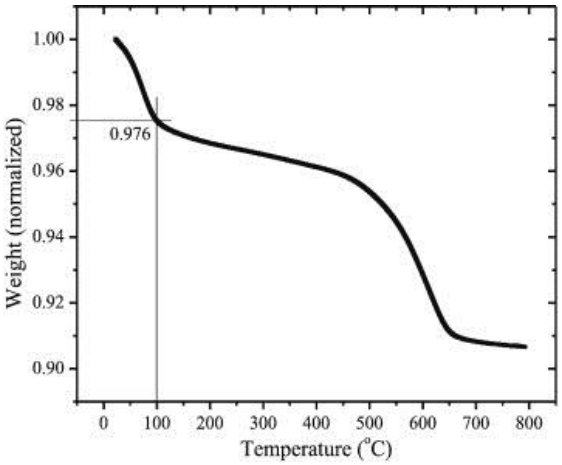

Fig. 1: Normalized weight of MMT while heated from 20 to 800 °C at a heating rate of 20 °C/min.

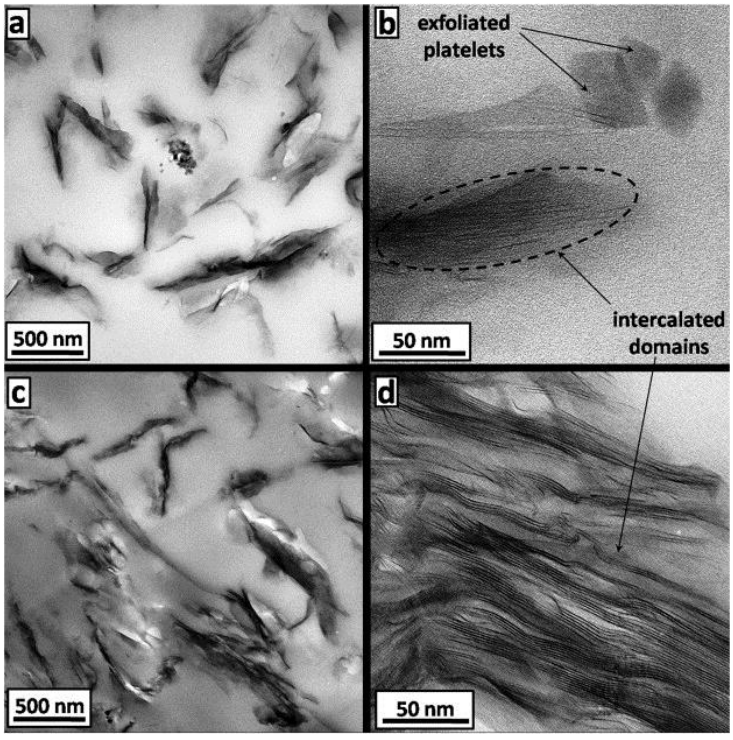

Fig. 2: TEM images of 5MMT (a and b) and 10MMT (c and d).

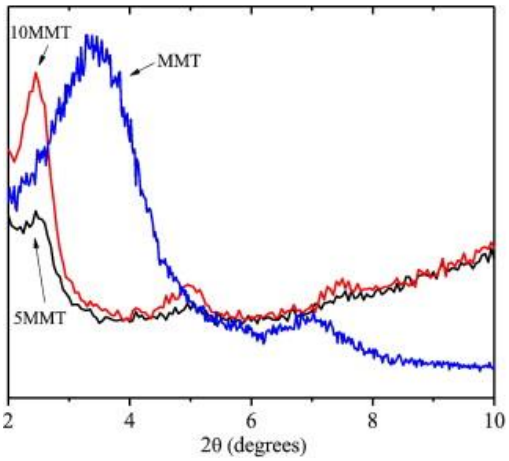

Fig. 3: XRD spectra of 5MMT, 10MMT and pure MMT.

As shown in Fig. 4, the real relative permittivity of the nanocomposite samples increases with temperature over the entire frequency range. At each temperature, the real relative permittivity of 10MMT is higher than that of 5MMT as a result of MMT's relative permittivity being higher than that of PMMA, coupled with an enhancement of interfacial polarization and electrical conduction with increasing MMT content. The imaginary relative permittivity is shown in Fig. 5. It is observed that the peaks of the β-relaxation of the two nanocomposites are located at higher frequencies, the assignment to the β-relaxation being made by comparison to the spectra for pure PMMA and by reference to the literature [4]. This figure also reveals that the strength of conduction increases with temperature and increasing MMT content. Above T_g, MWS- and α-relaxations occur between 0.01 and 100 Hz and are obscured by conduction effects in the nanocomposite samples. The measured permittivity data were used to model frequency dependence of dielectric relaxations and low-frequency conduction based on Havriliak–Negami and power-law terms [17], which will be described in the next section.

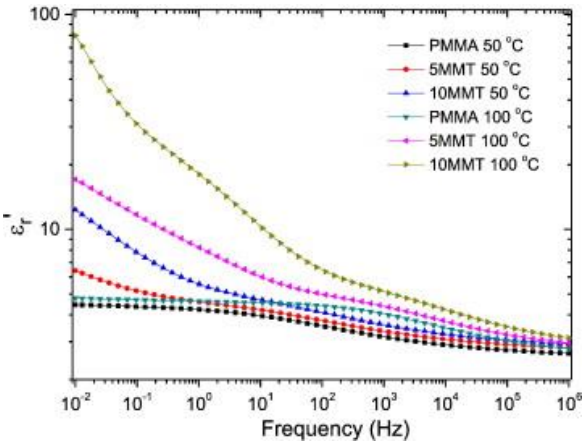

Fig. 4: The real relative permittivity of PMMA, 5MMT and 10MMT as a function of frequency at 50 and 100 °C. For clarity, only these two (out of thirteen) measured temperatures in the range from 30 to 140 °C, at 10 °C increments, are plotted here.

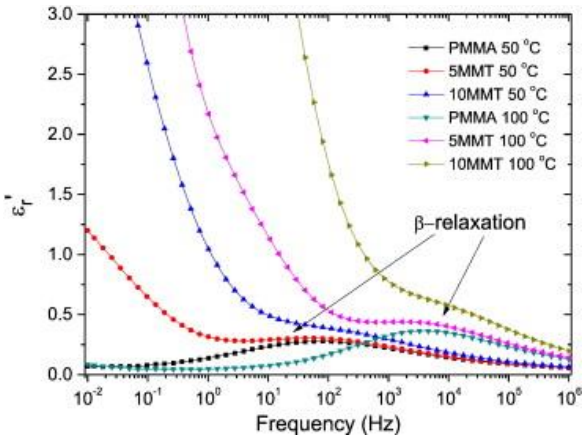

Fig. 5: The imaginary relative permittivity of PMMA, 5MMT, and 10MMT as a function of frequency at 50 and 100 °C.

4. Calculation

In pure PMMA, two dielectric relaxations (α- and β-) were observed in the frequency range studied here, whereas three dielectric relaxations were observed in the PMMA/MMT nanocomposites: α-, β-, and MWS relaxations. In addition, low-frequency conduction was observed caused by the existence of free charge carriers. The observed low-frequency conductivity was much stronger in the nanocomposites than in pure PMMA due to enhanced ionic electrical conduction from the ions in MMT. Since these four spectral phenomena commonly overlap at the temperatures studied here [4], among various models of the relaxation spectrum calculation [18] and [19], parametric functions describing dielectric relaxation and conduction were employed in order to separate them and facilitate analysis of their temperature- and frequency-dependence. An example of the parametric fit obtained for 5MMT at 50 °C (below T_g) is shown in Fig. 6. An example of the parametric fit obtained for 5MMT at 100 °C (above T_g), including the α-relaxation, is shown in Fig. 7.

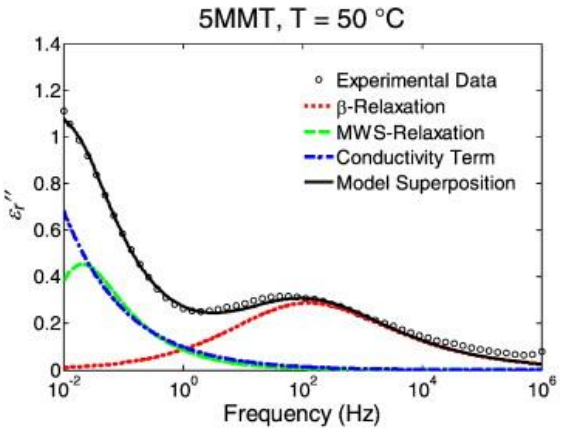

Fig. 6: Model fitting of the imaginary relative permittivity of 5MMT at 50 °C.

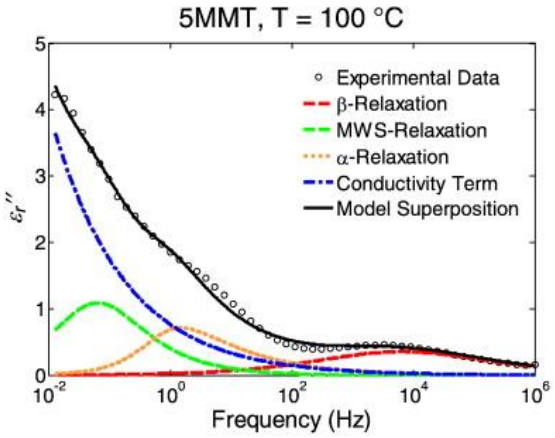

Fig. 7: Model fitting of the imaginary relative permittivity of 5MMT at 100 °C.

Classically, four relaxation functions have been developed and widely applied to describe dielectric relaxation: Debye [20], Cole–Cole [21], Davidson–Cole [22], and Havriliak–Negami (HN) [23] functions. Out of these four, the HN function, Eq. (2), is the most general because of its ability to model a broad and asymmetric distribution of relaxation times and it is employed in the following analysis,

$$\frac{\varepsilon_r^* - \varepsilon_{r\infty}}{\Delta\varepsilon_r} = \left\{1 + [i\omega\tau_0]^{1-a}\right\}^{-b}.$$

In Eq. (2), ε_r* is the complex relative permittivity; $\varepsilon_{r\infty}$ is the real relative permittivity caused by all processes with higher response rates than the particular mechanism under consideration; $\Delta\varepsilon_r$ is the dielectric strength of the relaxation process under consideration; τ_0 is the characteristic relaxation time, which depends on temperature; and *a* and *b* are two HN (shape) parameters that can be determined experimentally. The first HN parameter, *a*, is a measure of the peak height of the dielectric relaxation: as *a* increases, the peak height decreases. The second HN parameter, *b*, is one measure of the width of the distribution of relaxation times for asymmetric peaks. Note that for $a = 0$ and $b = 1$ the Debye model is recovered. The relationship between *a* and *b* is discussed in the original work [23] and subsequent texts, for example [24] and [25]. Briefly, $a > 0$ and $b \leq 1$ although *b* may be greater than unity if $ab \leq 1$.

Considering the contribution of free charge carriers to the low frequency behavior of imaginary permittivity, a power-law conductivity term is added to the HN functions in order to fully model the frequency dependence of the imaginary relative permittivity [17],

$$\varepsilon_r'' = A\omega^{-s} + \sum_{i=1}^{3}\left(\varepsilon_r''\right)_i.$$

In Eq. (3), *A* indicates the conduction strength, *s* is an exponent that always lies between 0 and 1, and $i = 1, 2, 3$ denotes the three relaxation processes: MWS, α - and β -. HN equations are normally applied to fit the imaginary part of complex relative permittivity directly collected from

experimental data. Imaginary permittivity curves can be easily overpowered, however, by rapidly increasing values as frequency is lowered, due to the conductive contribution of MMT free charge carriers. To counteract this effect, an alternative expression of the imaginary permittivity is implemented in this study in terms of the derivative of the real relative permittivity. The relation between the imaginary part and the real part is shown in Eq. (4) (which works for Debye relaxations). This expression is also applicable for Havriliak–Negami modeling since it can be decomposed into a series of Debye relaxations [25].

$$\frac{\partial \varepsilon_r'}{\partial \log \omega} = -\frac{\pi}{2}\varepsilon_r''$$

The criterion for a good fit between modeled permittivity and experimental data is to achieve a small least squares difference between the experimental data and the superposed HN functions, describing the dielectric relaxations and power-law conductivity term. The following procedure was used in this work to obtain the best parametric fit between the model of Eq. (3), with imaginary permittivity computed from real permittivity via Eq. (4) and the measured data. Below the glass transition temperature, the β-relaxation is well-separated from other relaxation processes in the dielectric frequency spectrum, shown by both 5MMT 50 °C and 10MMT 50 °C curves in Fig. 5. For this reason, the β-relaxation was fitted first by an HN function. Note that, although the β-relaxation is commonly symmetric in many polymers and in those cases can be successfully modeled using the Cole–Cole function (b = 1), in PMMA the β-relaxation is broadened asymmetrically [4] and the HN function is appropriate. Then, using the parametric fit to the β-relaxation, its effect in the frequency range 0.01 to 50 Hz was subtracted from the data in order to model the MWS relaxation. The peaks of the MWS relaxation are observed in this study to lie between 0.01 to 50 Hz. Similarly, using the parametric fit to the MWS relaxation, its effect was subtracted from the data in order to model the conductivity term. Once this initial fit was obtained for these three processes that occur below T_g, the fitting parameters were refined by making small adjustments (0.001 increments) in their values and seeking the minimum in the least squares difference between the experimental data and the model represented by Eq. (3). This fitting procedure was conducted for PMMA, 5MMT, and 10MMT at all temperatures studied (30 to 140 °C in 10 °C increments), with example fits shown in Fig. 6 and Fig. 7. Above T_g, the α-relaxation was modeled after initial parameters for the other three processes (mentioned above) had been determined. Fitting parameters were then iteratively refined as described above. The superposed HN functions agree well with the experimental data by showing a small sum of square difference. According to Eq. (5), the standard errors of curve fitting are 0.017 and 0.178 for 5MMT at 50 °C (Fig. 6) and 100 °C (Fig. 7). Dielectric spectra at other temperatures are fitted with similar standard errors. The values of the dielectric strength, $\Delta\varepsilon$, will be discussed in detail in the Discussion section, along with the effect of increasing MMT nanofiller content on dielectric properties of the composites.

$$\sum_i \left[\frac{\partial \varepsilon_{r\,exp}'(\omega_i)}{\partial \log \omega_i} - \left(A\omega^{-s} + \sum_{p=1}^{3} \frac{\partial \varepsilon_{r\,p}'(\omega_i)}{\partial \log \omega_i} \right) \right]^2 \rightarrow \min.$$

5. Discussion

5.1. Dielectric relaxations

Maximum frequencies, f_{max}, of α-, β-, and MWS relaxations as functions of reciprocal temperature are plotted as an Arrhenius diagram in Fig. 8. In the Havriliak–Negami model, the maximum frequency of each dielectric relaxation is obtained by modifying their parameters (*a*, *b*, and f_{HN}) in the HN model, according to Eq. (6) [26] and [27]. *a* and *b* are two HN (shape) parameters and f_{HN} is the characteristic frequency of relaxations.

$$f_{max} = f_{HN}\left\{\frac{\sin\left[\frac{\pi(1-a)b}{2(b+1)}\right]}{\sin\left[\frac{\pi(1-a)}{2(b+1)}\right]}\right\}^{-1/(1-a)}$$

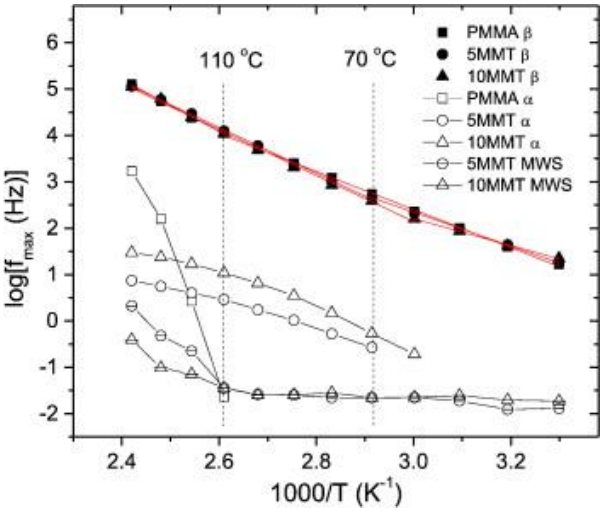

Fig. 8: Arrhenius diagram showing α -, β -, and MWS relaxations of PMMA, 5MMT, and 10MMT.

One important reason for plotting the maximum frequency of the dielectric relaxations of the samples is in order to determine their glass transition temperatures (T_g). The observation of the α-relaxation, Fig. 8, provides one measure of T_g for these samples. T_g was also determined by DSC, Fig. 9, to be the temperature at the maximal negative slope of the curves of heat flow versus temperature. No crystallization is observed in this amorphous PMMA system.

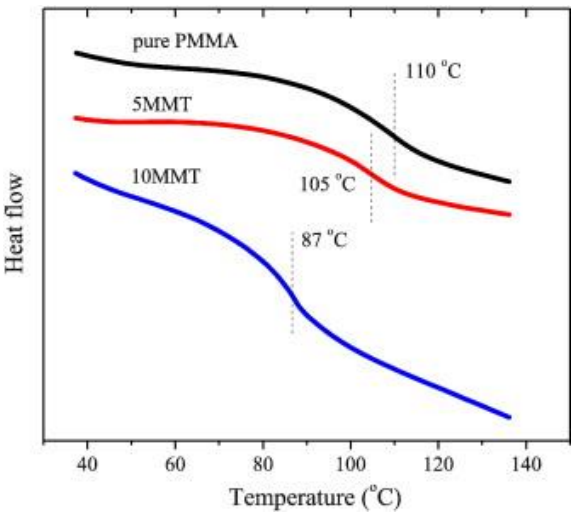

Fig. 9: DSC thermogram of PMMA and nanocomposites.

T_g obtained by dielectric spectroscopy and by DSC is listed in Table 2 for all of the samples. It is observed that T_g values for pure PMMA, measured by DSC and by dielectric spectroscopy, agree with each other. On the other hand, T_g values measured by DSC on the nanocomposites are significantly higher than those measured by dielectric spectroscopy. T_g from dielectric spectra is here determined as the particular temperature at which the addition of an α-relaxation peak improves the fitting to the observed spectra. This temperature is taken to be the lower limit of T_g. DSC-determined T_g is, on the other hand, a median value of T_g. Despite the discrepancy in the absolute value of T_g determined by the two methods, both show a trend of decreasing T_g as MMT content increases indicating a plasticizing effect of MMT on PMMA in these samples. Further, for PMMA/MMT nanocomposites, the maximum frequency of the α-relaxation increases with the MMT concentration at each temperature. This behavior is attributed to the segregation of PMMA polymer chains into smaller domains by silicate layers in MMT, enabling the α-relaxation to take place at lower temperatures and higher frequencies [13]. This is consistent with earlier results showing temperature dependence of T_g for nylon 6 and epoxy matrix nanocomposites with more than 4 wt.% MMT nanoclay [28], [29] and [30]. It is noteworthy that the maximum frequency of the α-relaxation of pure PMMA shifts more significantly than that of the nanocomposites when temperature changes. The α-relaxation occurs at a frequency much lower than that of the nanocomposites at 110 °C while its maximum frequency is two orders of magnitude higher than that of the nanocomposites at 140 °C. It is supposed that the MMT plays a similar role as the crystalline lamellae in copolymers [16], acting to segregate polymer chains, which slows down the α-relaxation. The dielectric strength of the α-relaxation is much higher in the nanocomposites than in pure PMMA, which will be discussed in the next section. Further, the role of MMT in constraining PMMA chains by intercalation is a possible contribution to the decrease in maximum frequency of α-relaxation in the nanocomposites, when compared with that of PMMA. The reciprocal temperature dependence of the maximum frequency of the α-relaxation follows the Vogel–Fulcher law [16], [26] and [31]:

$$f_{max} = f_0 e^{-\frac{DT_0}{(T-T_0)}}$$

where D is the strength parameter and T_0 is the Vogel temperature. It is stated in reference [32] that T_0 is usually between 30 and 70 K lower than T_g. In this case, when T_0 is 70 K (for 5MMT) and 60 K (for 10MMT) lower than T_g, i.e. when T_0 = 273 K, the linear relationships shown in Fig. 10 are obtained. D values for 5MMT and 10MMT are 0.87 ± 0.09 and 0.75 ± 0.08, resulting in no significant difference of temperature dependence for α-relaxation in 5MMT and 10MMT.

Table 2.
T_g of PMMA and of PMMA/MMT nanocomposites measured by DSC and by dielectric spectroscopy.

	PMMA	5MMT	10MMT
T_g (°C) — dielectric spectroscopy	110 ± 2	70 ± 2	60 ± 2
T_g (°C) — DSC	110 ± 1	105 ± 1	87 ± 1

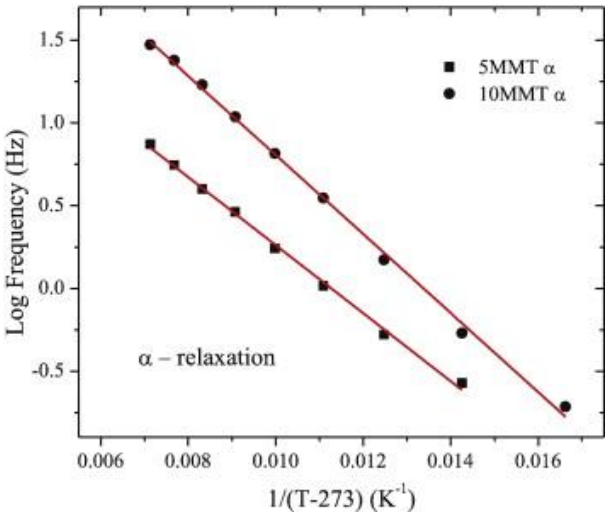

Fig. 10: The linear dependence of log f of α-relaxation of 5MMT and 10MMT on 1/(T-273).

It is observed from Fig. 8 that the maximum frequency of the β-relaxation does not shift significantly with the addition of MMT. Further, the β-relaxation of PMMA, 5MMT, and 10MMT follows a linear relationship between log frequency and the reciprocal of temperature, as Fig. 8 shows, indicating that the β-relaxation obeys the Arrhenius law:

$$f_{max} = f_0 e^{\frac{-E_a}{RT}}$$

where f_{max} is the maximum frequency, T is the temperature, f_0 is a phenomenological parameter, E_a is the activation energy of the dielectric relaxation, and R is the universal gas constant. Linear fits to the β-relaxation data are shown in Fig. 8 by solid lines and activation energies deduced from these are listed in Table 3. An increase of activation energy for the β-relaxation occurs above T_g as a result of coupling between the α-relaxation and the localized β-relaxation [33] and [34]. On the other hand, the activation energy of the β-relaxation decreases on addition of MMT, both above and below T_g.

Table 3.
Activation energy of the β-relaxation of PMMA and PMMA/MMT nanocomposites obtained by dielectric spectroscopy.

Sample	E_a (kJ/mol), $T < T_g$	E_a (kJ/mol), $T > T_g$
PMMA	79 ± 4	107 ± 5
5MMT	70 ± 4	94 ± 5
10MMT	55 ± 3	95 ± 5

Referring again to Fig. 8, MWS relaxation is observed only in the dielectric spectra of 5MMT and 10MMT, attributed to the interfacial effect of MMT platelets. Below 110 °C, the maximum frequency of the MWS relaxation is independent of temperature. This implies that the number of free charges participating in MWS relaxation is not increased by increasing temperature, when the material is in the glassy state. The shift of the relaxation peak to higher frequencies occurs in both 5MMT and 10MMT above 110 °C, however, indicating the increase of the aptitude of the ions to participate in interfacial polarization with the increase in MMT content [35] when the polymer is in the rubbery state. Similar temperature dependence of MWS relaxation above T_g has been reported by other researchers [13], [35] and [36].

5.2. Dielectric strength

The dielectric strength of the dielectric relaxations, $\Delta\varepsilon$, is plotted against the reciprocal of temperature in Fig. 11, Fig. 12 and Fig. 13 for β-, α-, and MWS relaxations, respectively. A 5% uncertainty is applied to every data point to reflect the overall uncertainty in the experiment and model fitting method [26]. Fig. 11 reveals that the relaxation strength of the β-relaxation does not change significantly with MMT content. This reflects the fact that the β-relaxation is related to the rotation of the side ester group. Fig. 12 indicates that the strength of α-relaxations increases with respect to a higher MMT loading, which is supposedly caused by looser molecular packing of the polymer chains, triggered by the presence of the nanoclay [37]. For each MMT loading, the strength of the α-relaxation increases with respect to temperature until approximately 120 °C, after which it slightly decreases. The peak in $\Delta\varepsilon$ for α- and MWS relaxations at T_g in 5MMT and 10MMT (Fig. 12 and Fig. 13) suggests that there is possible cooperation between the MWS relaxation and the α-relaxation above T_g since the frequency range of α- and MWS relaxations is getting close.

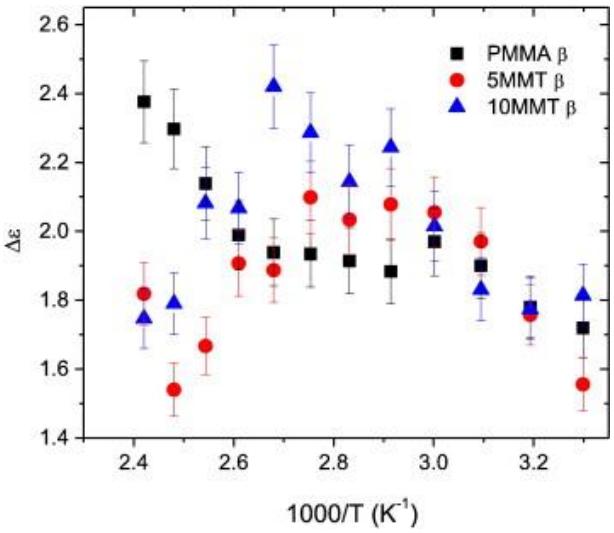

Fig. 11: $\Delta\varepsilon$ of the β-relaxation of PMMA, 5MMT, and 10MMT as a function of reciprocal temperature.

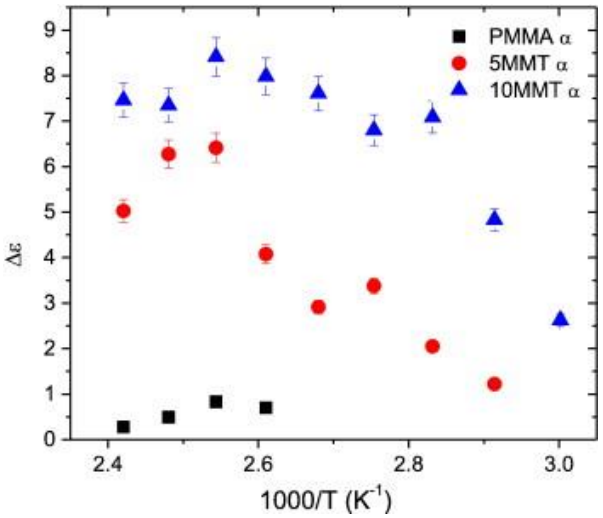

Fig. 12: $\Delta\varepsilon$ of the α-relaxation of PMMA, 5MMT, and 10MMT as a function of reciprocal temperature.

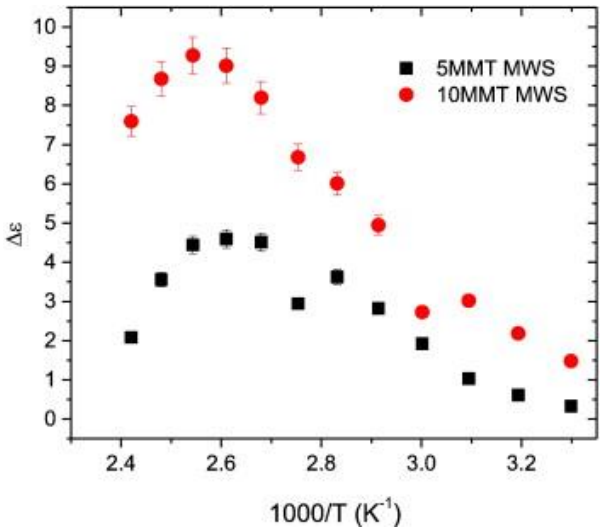

Fig. 13: $\Delta\varepsilon$ of the MWS relaxation of 5MMT and 10MMT as a function of reciprocal temperature.

6. Conclusions

Dielectric relaxation dynamics of PMMA/MMT nanocomposites have been modeled using parametric functions. The model superposition shows a good fit to experimental data at all measured temperatures. It is observed that the glass transition (α-relaxation) of PMMA takes place at lower temperatures as MMT content increases, because the polymer chains are segregated into smaller domains by the silicate layers of MMT. The maximum frequency and activation energy of the β-relaxation decrease with increasing MMT content. On the other hand, the maximum frequency of the MWS relaxation starts increasing significantly above 110 °C. The dielectric strength of the β-relaxation shows a weak temperature and frequency dependence whereas the dielectric strength of α - and MWS relaxations is significantly increased with increasing MMT content.

Acknowledgments

This work was supported by NASA (Cooperative Agreement No. NNX09AP70A).

References

[1] T. Tanaka. Dielectric nanocomposites with insulating properties. IEEE Trans. Dielectr. Electr. Insul., 12 (2005), pp. 914–928.

[2] J.W. Gilman, T. Kashiwagi, J.D. Lichtenhan. Nanocomposites: a revolutionary new flame retardant approach. SAMPE J., 33 (1997), pp. 40–46.

[3] F. Bellucci, D. Fabiani, G.C. Montanari, L. Testa. The processing of nanocomposites. J.K. Nelson (Ed.), Dielectric Polymer Nanocomposites, Springer, New York (2010), p. 31.

[4] R. Bergman, F. Alvarez, A. Alegria, J. Colmenero. The merging of the dielectric alpha- and beta-relaxations in poly(methyl methacrylate). J. Chem. Phys., 109 (1998), pp. 7546–7555.

[5] M.S. Ardi, W. Dick, J. Kubat. Time-domain dielectric-relaxation of poly(methyl methacrylate) and nitrile rubber. Colloid Polym. Sci., 271 (1993), pp. 739–747.

[6] J. Colmenero, A. Alegria. Methyl group dynamics in glassy polymers by neutron scattering: from classical to quantum motions. Adv. Funct. Mol. Polym., 2 (2001), pp. 271–294

[7] V.M. Boucher, D. Cangialosi, A. Alegria, J. Colmenero, J. Gonzalez-Irun, L.M. Liz-Marzan. Physical aging in PMMA/silica nanocomposites: enthalpy and dielectric relaxation. J. Non-Cryst. Solids, 357 (2011), pp. 605–609.

[8] P.S. Gill, C.L. Marcozzi, I.F. Groves. Dielectric Materials, Measurements and Applications. Institution of Engineering and Technology, Manchester (1992), p. 429.

[9] X. Yi, H.L. Duan, Y. Chen, J. Wang. Prediction of complex dielectric constants of polymer–clay nanocomposites. Phys. Lett. A, 372 (2007), pp. 68–71.

[10] C.V. Chanmal, J.P. Jog. Study of dielectric behavior in PVDF/clay nanocomposites. e-Polymers (1, 2009).

[11] M. Kato, A. Usuki. Polymer–Clay Nanocomposites. T.J. Pinnavaia, G.W. Beall (Eds.)Wiley, West Sussex (2000).

[12] N. Fuse, T. Tanaka, Y. Ohki. IEEE, evaluation of dielectric properties in polypropylene/clay nanocomposites. Ceidp: 2009 Annual Report Conference on Electrical Insulation and Dielectric Phenomena, Ieee, New York (2009), pp. 35–38

[13] Y.H. Lee, A.J. Bur, S.C. Roth, P.R. Start. Accelerated alpha relaxation dynamics in the exfoliated nylon-11/clay nanocomposite observed in the melt and semicrystalline state by dielectric spectroscopy. Macromolecules, 38 (2005), pp. 3828–3837

[14] Y.H. Lee, A.J. Bur, S.C. Roth, P.R. Start, R.H. Harris. Monitoring the relaxation behavior of nylon/clay nanocomposites in the melt with an online dielectric sensor. Polym. Adv. Technol., 16 (2005), pp. 249–256.

[15] M. Encinar, E. Guzman, M.G. Prolongo, R.G. Rubio, C. Sandoval, F. Gonzalez-Nilo, L. Gargallo, D. Radic. Dielectric and dynamic-mechanical study of the mobility of poly(t-butylacrylate) chains in diblock copolymers: polystyrene-b-poly(t-butylacrylate). Polymer, 49 (2008), pp. 5650–5658

[16] S. Moreno, R.G. Rubio. Dielectric study of the dynamics of poly(oxyethylene) chains in triblock copolymers: poly(oxyethylene)-b-polystyrene-b-poly(oxyethylene). Macromolecules, 35 (2002), pp. 5483–5490

[17] E. Schlosser, A. Schonhals. Recent development in dielectric-relaxation spectroscopy of polymers. Colloid Polym. Sci., 267 (1989), pp. 963–969

[18] Y.N. Huang, Y.N. Wang, E. Riande. A dynamically heterogeneous coupled dissipation scenario of glass transition. J. Chem. Phys., 111 (1999), pp. 8503–8509

[19] M. Encinar, M.G. Prolongo, R.G. Rubio, F. Ortega, A. Ahmadi, J.J. Freire. Dielectric and molecular dynamics study of the secondary relaxations of poly(styrene-co-methylmethacrylate) copolymers: influence of the molecular architecture. Eur. Phys. J. E, 34 (2011)

[20] P. Debye. Some results of kinetic theory of isolators. (preliminary announcement). Phys. Z., 13 (1912), pp. 97–100.

[21] K.S. Cole, R.H. Cole. Dispersion and absorption in dielectrics I. Alternating current characteristics. J. Chem. Phys., 9 (1941), pp. 341–351.

[22] D.W. Davidson, R.H. Cole. Dielectric relaxation in glycerol, propylene glycol, and normal-propanol. J. Chem. Phys., 19 (1951), pp. 1484–1490.

[23] S. Havrilia, S. Negami. A complex plane representation of dielectric and mechanical relaxation processes in some polymers. Polymer, 8 (1967), p. 161.

[24] Y.N. Huang, C.J. Wang, E. Riande. Superdipole liquid scenario for the dielectric primary relaxation in supercooled polar liquids. J. Chem. Phys., 122 (2005).

[25] M. Wubbenhorst, J. van Turnhout. Analysis of complex dielectric spectra. I. One-dimensional derivative techniques and three-dimensional modelling. J. Non-Cryst. Solids, 305 (2002), pp. 40–49

[26] J. Liu, H.Z. Guo, X.C. Pang, X.L. Tan, M. Akinc, Z.Q. Lin, N. Bowler. Dynamics of polystyrene-block-poly(methylmethacrylate) (PS-b-PMMA) diblock copolymers and PS/PMMA blends: a dielectric study. J. Non-Cryst. Solids, 359 (2013), pp. 27–32.

[27] R. Diaz-Calleja. Comment on the maximum in the loss permittivity for the Havriliak–Negami equation. Macromolecules, 33 (2000), p. 8924-8924.

[28] O. Becker, R. Varley, G. Simon. Morphology, thermal relaxations and mechanical properties of layered silicate nanocomposites based upon high-functionality epoxy resins. Polymer, 43 (2002), pp. 4365–4373.

[29] L. Wang, K. Wang, L. Chen, Y.W. Zhang, C.B. He. Preparation, morphology and thermal/mechanical properties of epoxy/nanoclay composite. Compos. A Appl. Sci. Manuf., 37 (2006), pp. 1890–1896.

[30] N. Noda, Y.H. Lee, A.J. Bur, V.M. Prabhu, C.R. Snyder, S.C. Roth, M. McBrearty. Dielectric properties of nylon 6/clay nanocomposites from on-line process monitoring and off-line measurements. Polymer, 46 (2005), pp. 7201–7217.

[31] H. Vogel. The temperature dependence law of the viscosity of fluids. Phys. Z., 22 (1921), pp. 645–646.

[32] G.R. Strobl. Physics of Polymers (second ed.)Springer, New York (1996).

[33] Y. Wang, W.C. Chen. Dielectric probing of relaxation behaviors in pmma/organoclay nanocomposites: effect of organic modification. Compos. Interfaces, 17 (2010), pp. 803–829

[34] X. Jin, S.H. Zhang, J. Runt. Broadband dielectric investigation of amorphous poly(methyl methacrylate)/poly(ethylene oxide) blends. Macromolecules, 37 (2004), pp. 8110–8115

[35] H. Hammami, M. Arous, M. Lagache, A. Kallel. Study of the interfacial MWS relaxation by dielectric spectroscopy in unidirectional PZT fibres/epoxy resin composites. J. Alloys Compd., 430 (2007), pp. 1–8

[36] G.A. Kontos, A.L. Soulintzis, P.K. Karahaliou, G.C. Psarras, S.N. Georga, C.A. Krontiras, M.N. Pisanias. Electrical relaxation dynamics in TiO(2)–polymer matrix composites. Express Polym. Lett., 1 (2007), pp. 781–789.

[37] D. Fragiadakis, E. Logakis, P. Pissis, V.Y. Kramarenko, T.A. Shantalii, I.L. Karpova, K.S. Dragan, E.G. Privalko, A.A. Usenko, V.P. Privalko. Polyimide/silica nanocomposites with low values of dielectric permittivity. A.G. Nassiopoulou, N. Papanikolaou, C. Tsamis (Eds.), Second Conference on Microelectronics, Microsystems and Nanotechnology, IOP Publishing Ltd, Bristol (2005), pp. 139–142.